Journal of Electronic Materials
https://doi.org/10.1007/s11664-026-12860-8

ORIGINAL RESEARCH ARTICLE

The Impact of Phenanthroimidazole-Imine Dye on Photovoltaic Performance of Semiconductor/Insulator/Semiconductor (SIS)-Type Solar Cells

Songül Fiat Varol[1] · Sibel Gülle[2] · Seçil Çelik Erbaş[3] · Ziya Merdan[4]

Received: 14 December 2025 / Accepted: 1 April 2026
© The Author(s) 2026

Abstract
The purpose of this study is to analyze the photovoltaic (PV) parameters of TiO_2/CN-i/SiO_2/*p*-Si and TiO_2/SiO_2/*p*-Si semiconductor/insulator/semiconductor (SIS) solar cells (SCs). The organic semiconductor selected was the phenanthroimidazole-imine derivative (CN-i). The TiO_2 thin film showed the anatase phase, with (101) and (004) characteristic reflections in x-ray diffraction (XRD) measurements. The optical bandgaps of TiO_2 and CN-i thin films are calculated as 3.38 eV and 2.76 eV from UV–Vis spectra. To characterize the PV properties, the samples are irradiated through the transparent TiO_2/CN-i double layers, and the parameters are obtained from J–V (current density–voltage) measurements in dark and under different illumination intensities; 10 mW/cm^2, 15 mW/cm^2, 25 mW/cm^2, 50 mW/cm^2, 100 mW/cm^2. The current density increased considerably, ensuring a good PV conversion. Fill factor (FF) also increased from 55.12% to 69.10 % after inserting the CN-i dye under 100 mW/cm^2 illumination. Also, the ionization energy level, electron affinity, and photoconductivity values are obtained by photoemission yield spectroscopy and photoconductivity measurements. Transient photocurrent plots are analyzed and the device illuminated at 100 mW/cm^2 demonstrates an outstanding power conversion efficiency (PCE) of 18.24% with supported incident photon-to-current efficiency (IPCE) data and transient photocurrent traces in the same conditions.

Keywords Phenanthroimidazole-imine derivatives · organic solar cell (OSC) · photoelectrical characterization · SIS structures

Introduction

Organic π-conjugated compounds have recently attracted significant interest in optoelectronic research owing to their easily tunable photophysical and electrochemical characteristics as well as the availability of practical synthetic routes.[1] Establishing clear correlations between molecular structures and resulting properties is essential to developing materials that exhibit desirable optical, electrochemical, and thermal behaviors, which are crucial for applications in organic light-emitting diodes (OLEDs),[2–5] organic photovoltaics (OPVs),[6] organic field-effect transistors (OFETs),[7] molecular sensors, and nonlinear optical devices.[8] Although phenanthroimidazole derivatives have been extensively investigated for OLED applications, their potential for photovoltaic purposes has been largely overlooked, with the majority of research remaining OLED-centered.[9–15]

In this study, we introduce a new semiconductor–insulator–semiconductor (SIS) solar cell (SC) design that integrates organic semiconductors with inorganic counterparts. Compared with Schottky or MIS architecture, SIS structures are more stable and typically provide superior performance. This improvement arises from the suppression of majority carrier tunneling, the elimination of thin metallic layers that not only absorb incident light but also degrade mechanically, and the ability to select wide conductivity ranges and suitable bandgaps in the top layer. Moreover, the top

✉ Songül Fiat Varol
songulvfiat@yahoo.com

1 Vocational School of Technical Sciences, Electric and Energy Department, Manisa Celal Bayar University, 45140 Manisa, Turkey

2 Faculty of Arts and Sciences, Department of Chemistry, Manisa Celal Bayar University, 45140 Manisa, Turkey

3 Faculty of Engineering, Department of Metallurgy and Materials Engineering, Manisa Celal Bayar University, 45140 Manisa, Turkey

4 Faculty of Arts and Sciences, Physics Department, Gazi University, 06500 Ankara, Turkey

Published online: 16 April 2026

semiconductor thin film functions simultaneously as an antireflection coating, a transparent window with low series resistance, and an effective charge-collecting layer.[16]

The diffusion process commonly employed in conventional solar cell production is complicated, requiring both high processing temperatures and significant costs. In contrast, Schottky solar cells can be fabricated at relatively low temperatures and with reduced expenditure. In such devices, two critical factors govern performance: the difference in work function between the base semiconductor and the metal or TCO contact, and the thickness of the interfacial layer, since electron transport across this interface proceeds mainly by tunneling.[17] The operating principle of the SIS structure is depicted in Fig. 1, where the thickness of the front layer—here titanium dioxide (TiO_2) and the organic dye 4-(1-butyl-1H-phenanthro[9,10-d]imidazol-2-yl)-N-(4-cyanobenzylidine)aniline (CN-i)—plays a decisive role in the extent of solar radiation absorption, being governed by both absorption and reflection phenomena. Optimal thickness values must be chosen for these front layers so as to minimize reflectance in the spectral region corresponding to the highest sensitivity of the $TiO_2/SiO_2/Si$ solar cell.

The overall performance of SIS devices depends strongly on the thickness of the insulating SiO_2 film located at the TCO–Si interface. This interlayer enhances the barrier height of the junction while simultaneously lowering the saturation current. To enable efficient tunneling of charge carriers, the SiO_2 film must be sufficiently thin and electrically transparent; in practice, its thickness should not exceed a few tens of angstroms.[18–22] The choice of SiO_2 as a buffer layer is motivated by three advantages: (i) thermally grown SiO_2 on silicon forms a natural oxide with low interface state density ($<1\times10^{10}$ cm^{-2} eV^{-1}), (ii) the SiO_2 surface provides an excellent template for the deposition of organic thin films such as CN-i, and (iii) the insulating properties of SiO_2 help suppress carrier recombination at the interface while enhancing the device's photoconductive response.

Within this framework, TiO_2 is widely utilized as a wide-bandgap semiconductor in ultraviolet photodetectors; however, its use in visible photodetection remains limited.[23,24] Several strategies have been reported to reduce the bandgap of TiO_2, including dye or quantum dot sensitization,[25] cation/metal/anion doping,[26] ion implantation,[27] and heterojunction engineering.[28] Silicon, with its narrow bandgap of 1.1 eV, and TiO_2, with a wide bandgap of about 3.2 eV,[29] form a contact that effectively reduces the overall optical bandgap. This aligns with the general principle that efficient solar absorbers should have a bandgap in the 1.0–1.7 eV range to capture a broad portion of the solar spectrum. Beyond bandgap considerations, however, effective solar absorbers must also support conduction pathways that minimize recombination losses.

In this context, the organic dye CN-i[30] was chosen for its ease of synthesis, structural stability, and favorable optoelectronic properties. CN-i exhibits strong intermolecular π–π stacking, a rigid coplanar backbone, and a symmetric molecular configuration, all of which enhance charge transport, reduce recombination, and stabilize carrier lifetimes. The cyano group acts as an effective bridge between donor and acceptor units, decreasing torsional angles and finely tuning the electronic properties of the chromophore.

When incorporated as the third layer in the SIS structure, CN-i provides an energy alignment mechanism by serving as a "staircase," guiding electron transfer across the device with improved control. With highest occupied molecular orbital (HOMO) and lowest unoccupied molecular orbital (LUMO) levels of 5.44 eV and 2.67 eV, respectively, CN-i enhances absorption and charge mobility while reducing

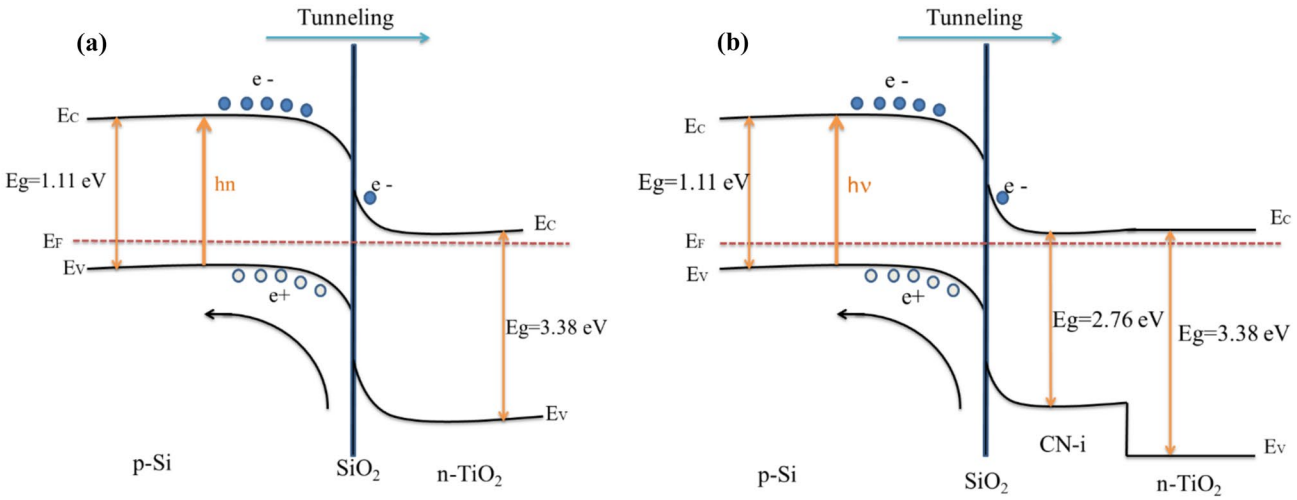


Fig. 1 Energy band diagram of (a) $TiO_2/SiO_2/p$-Si (b) TiO_2/ CN-i/SiO_2/p-Si heterojunction device.

recombination losses. Furthermore, the close work function compatibility of TiO_2 (3.38 eV) and CN-i (2.76 eV, both values derived from the onset of UV–Vis absorption spectra using Planck's relation)[15,16] establishes favorable band bending and improved carrier transport, leading to higher current conduction and better efficiency. This integration suppresses drawbacks such as insufficient absorption and short carrier lifetimes, resulting in a more robust photovoltaic response.

In the past few decades, the development of novel organic semiconductors incorporating long alkyl chains has advanced rapidly, enabling the design of new optoelectronic devices.[31–34] Among these, heteroaromatic five- and six-membered rings are particularly attractive as π-conjugated building blocks, acting as donors or acceptors and improving overall polarizability.[35–38] Within this context, imidazole-based systems are especially relevant owing to their intriguing optical and electrical properties arising from their conjugated chromophores. The imidazole ring contains two distinct nitrogen atoms that create chemically stable heterocycles with tunable electronic structures, allowing straightforward synthesis and functionalization.[39–41] In the present study, we employ a phenanthroimidazole-imine derivative (CN-i) as the donor material in SIS solar cells, which has been proposed as a cost-effective route for photovoltaic energy conversion.

Following more than two decades of limited exploration, SIS-type solar cells have regained attention as crystalline Si technologies approach their practical limits. In parallel, two-dimensional materials such as graphene have emerged as promising candidates for SIS devices, leading to demonstrations of graphene-based[42] and ZnO-based[43] SIS solar cells. Theoretical calculations predict that $ZnO/SiO_2/Si$ devices could achieve efficiencies as high as 25%,[44] stimulating the pursuit of advanced architectures including core–shell SIS configurations[45] and dye-sensitized approaches.[46,47] Jiang and co-workers, for example, reported significant improvements in ITO/ITOH/Si heterojunction solar cells fabricated by radio frequency (RF) magnetron sputtering, where hydrogen incorporation reduced resistance after annealing and raised the fill factor, yielding a maximum efficiency of 17.5%.[48] Similarly, efficiencies of 10.8% and 12.2% under AM0 and AM2 illumination, respectively, have been reported for ITO–SiO*x*–*n*-Si SIS devices.[49] Untila and colleagues[50–53] further demonstrated bifacial SIS/Si homojunctions with efficiencies up to 16.6%. More recently, an upper efficiency limit of 23.6% has been proposed for carrier-selective $ITO/SiO_2/Si$ SIS structures.[54]

Despite these advances, SIS solar cells are often limited by the relatively short lifespan of transparent conducting oxides and the large bandgaps of candidate materials. To overcome these barriers, researchers have sought to tune bandgaps in materials such as ZnO[55] and graphene,[56,57] while surface engineering techniques have been applied to reduce recombination velocities and extend minority carrier lifetimes.[58] For instance, Kumar et al. (2020)[59] reported MoS_2/AlN/Si heterojunctions in which an ultrathin AlN layer boosted device efficiency from 2.92% to 3.53% by suppressing static charge transfer and enabling improved Fermi level alignment. In parallel, strategies involving advanced TiO_2-based electrodes and molecular light collectors have introduced new design paradigms for next-generation photovoltaics.[60–63]

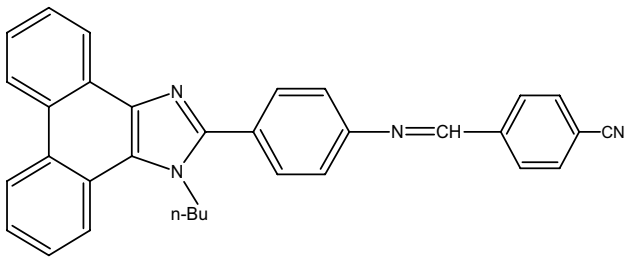
As reflected in these studies, fabrication of MIS and SIS devices is often simpler than that of diffused junctions. Nevertheless, these processes remain more complex than standard *p*–*n* junction technologies, and MIS/SIS configurations are not necessarily cost-effective unless fabricated using nonvacuum approaches. Moreover, their commercial viability depends on achieving device efficiencies competitive with diffused cells. Although theoretical efficiencies for MIS/SIS designs slightly exceed those of diffused junctions, experimentally reported values remain modest. Therefore, consistent realization of high efficiency remains a primary challenge. Further research into degradation mechanisms, interfacial oxide properties, conductive oxide reactions, and large-scale fabrication methodologies is essential to advance this field.

In the present work, we report a new phenanthroimidazole-imine dye (CN-i) designed for integration in SIS solar cells to enhance charge mobility, accelerate electron transport, and improve extraction efficiency. Our device configuration, TiO_2/CN-i/SiO_2/Si, is compared against a reference TiO_2/SiO_2/Si structure to assess the influence of CN-i on photovoltaic performance. We investigate how the HOMO–LUMO levels of CN-i alter charge transport under dark and illuminated conditions and evaluate their impact on key device parameters including fill factor, power conversion efficiency, incident photon-to-current conversion efficiency (IPCE), transient photocurrent, photoemission yield spectroscopy, and photoconductivity.

Experimental

Preparation of CN-i /SiO_2/Si Heterojunction

The Si substrate (size 7 mm × 7 mm) used in this work is a *p*-type semiconductor with resistivity of 10.4 Ω cm measured by Four-Point probes and a thickness of 500 µm. Before preparing the CN-i film, the molecular structure, given in Scheme 1, of the Si substrate was ultrasonically cleaned in sequence with acetone, ethanol, and deionized water, which retains the native oxide layer (~1.0 nm) over the Si surface. Then CN-i obtained from a homogeneous solution in chloroform (~10 mg/ml) organic film was deposited on the SiO_2 layer by the spin-coating method (1000 rpm, 60s) and dried



Scheme 1 Molecular structure of CN-i compound, data from Ref.30.

in a vacuum oven at 50°C for 24 h. The CN-i layer thickness was directly measured by spectroscopic ellipsometry prior to TiO_2 deposition. Ellipsometric measurements were performed on CN-i films deposited on Si/SiO_2 substrates under identical spin-coating conditions. In addition, the spin-coating process was monitored *in situ* using the built-in thickness monitoring system to ensure high reproducibility between samples. While ellipsometry provides effective optical thickness rather than a purely geometric one, this approach is well suited for ultrathin organic interlayers and is commonly employed in SIS device studies. The CN-i layer thickness (~3 nm) was kept approximately constant to emphasize its interfacial role rather than bulk absorption, and the selected deposition conditions were found to yield reproducible and near-optimal device performance.

TiO_2 thin films were deposited onto CN-i film (CN-i-TiO_2) by re-active magnetron sputtering in the High-Power Impulse Magnetron Sputtering (HiPIMS) mode in a single stage process from a 99.5% pure Ti target (300 mm × 100 mm) in an argon/oxygen atmosphere (3.0 sccm O_2 and 50 sccm Ar) at a pressure of 0.5 Pa. The oxygen flow rate was controlled by optical emission monitoring to provide stoichiometric TiO_2 (~60 nm thickness obtained with spectroscopic ellipsometry) coatings. The HiPIMS power was operated at 700 Hz pulse frequency with a 40 µs duration pulse and the voltage was set to 500 V. This resulted in a time averaged power at ~1.5 kW. The coatings were deposited on the CN-i film, which were ultrasonically pre-cleaned in propanol prior to deposition. The substrates were mounted on a rotating drum substrate holder (1 m circumference) that was electrically floating. The deposition time was ~1 h for the samples. Al back and Au (~700 nm) front contacts were obtained with reactive magnetron sputtering. The energy band diagrams of $TiO_2/SiO_2/p$-Si and TiO_2/ CN-i /SiO_2/p-Si heterojunction devices are shown in Fig. 1a, b.

Current density–voltage measurements were carried out in ambient air under AM 1.5G illumination using a self-calibrating Scientech model solar simulator, SL-60A-WS (On N6N1R3, Canada). An X200 source meter (Ossila, Sheffield, UK) was used to evaluate solar cell performance (scan speed 100 mV s^{-1}). A mask was used to limit the active solar cell area to 0.16 cm^2. Transient photocurrent measurements were performed at 293 K on an optimized device at short circuit and at an applied bias of −1 V.

Results and Discussion

Structural and Morphological Characterization

In order to investigate the structural properties of TiO_2 thin films, the XRD measurements was performed over the range 20°–80° and the spectra are presented in Fig. 2. It can be seen that the pure TiO_2 thin film was in the anatase crystal plane with (101) and (004) reflections, exhibiting characteristic peaks consistent with the JCPDS card no: 21-1272 (anatase TiO_2); (101) preferred orientation at $2\theta = 26.41^{\circ}$ and $2\theta = 36.33^{\circ}$. According to Scherrer's Equation ($D = O.9\lambda/\beta Cos\theta$),[64] the crystallite sizes (D) were obtained as 24.36 nm and 19.38 nm. The relative peak intensity shows a good crystallinity and planar organization to enable a good film growth over it. The inset shows the scanning electron microscopy (SEM) images (see Fig. 2) confirming that CN-i organic addition achieved a controlled all blended structural (TiO_2/CN-i) arrangement and uniform film morphology by inhibiting the disordered crystal growth and providing homogeneous nucleation sites. As we see from the SEM images, as the magnification ratio increases, the granular formation becomes more evident and more compact. The size of the crystallites seem to be in the sub-micrometer range and of the same order as was estimated by the x-ray diffraction (XRD) peaks. While this formation increases regularity, the film quality also increases. This will ensure better performance of the layers in device fabrication.

Phenanthroimidazoles containing an amino group form phenanthroimidazole imine compounds through the condensation of this amino group with various aldehyde derivatives. These compounds can be easily synthesized in a single step and obtained with high yields. The presence of donor and acceptor groups in the CN-i molecule, along with the high π electron density of the phenanthroimidazole ring used as the donor group, increases the electron mobility in the structure. Additionally, the high photostability of these compounds under UV light and their high Stokes shift values provide an advantage for their use in solar cells. The fact that they can be synthesized in a single step with simple aldehyde derivatives also reduces production costs. These features make phenanthroimidazole derivatives more attractive compounds compared with other phenanthroimidazole-based molecules in literature.

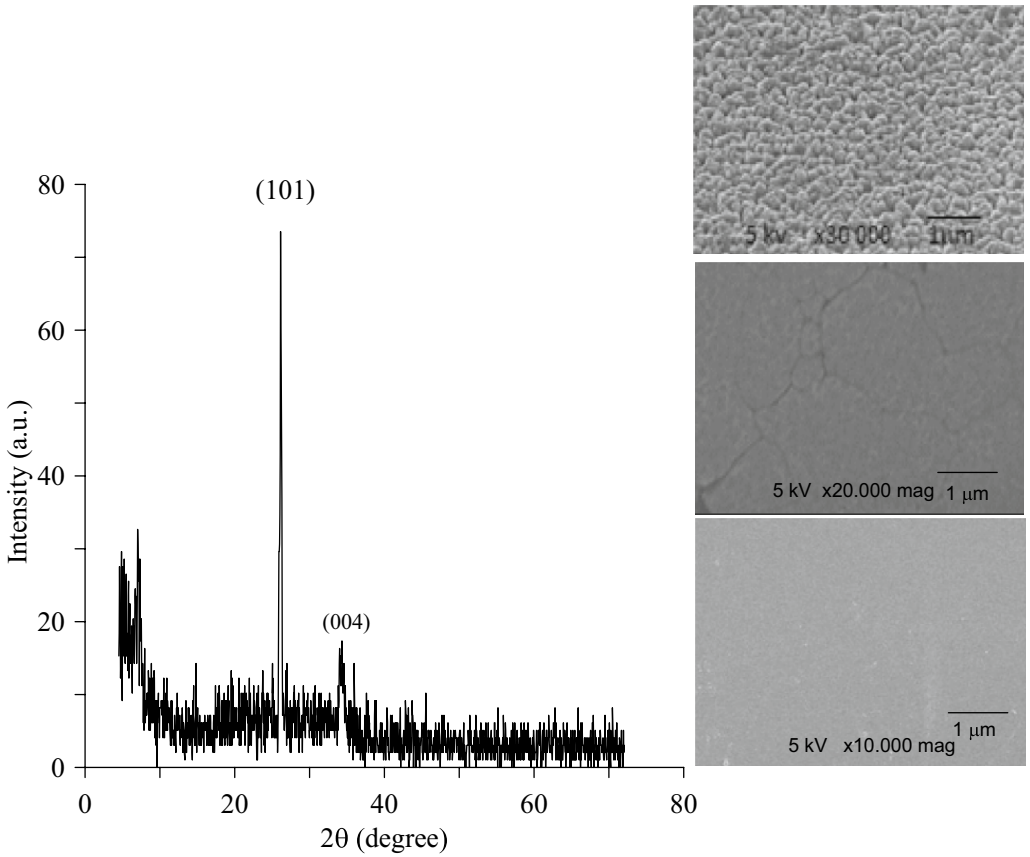


Fig. 2 X-ray diffraction patterns of TiO_2 thin films with inset scanning electron microscopy (SEM) image.

Photovoltaic Properties

The optical bandgaps of TiO_2 and CN-i thin film layers were obtained from the onset of UV–Vis absorption spectra by the Planck hypothesis formula as 3.38 eV (367 nm) and 2. 76 eV (450 nm), respectively (see Fig. 3). These values are key parameters to set an ideal energy balance for the structure of SIS SC device as exhibited in Fig. 1.

TiO_2 is an active material with high electron mobility and high photonic performance. PV performance is mostly promoted by its power-conversion efficiency (PCE) which is determined by many essences including light harvesting, the exciton diffusion length, and separation/transportation/collection by defined electrodes in SC design. Energy gap values mostly depend on the crystal structure of the film and also the positions and alignment of atoms in the crystal lattice and are inevitably affected by crystal disorder.

On the other hand, another issue we expect is CN-i to show a similar absorption compared with TiO_2. With their ideal optical properties, these two TiO_2 and CN-i contribute to the charge transmission by completing their works in this multi-structure correctly, and this is supported by detailed data below (Table I). By adding CN-i, the current density

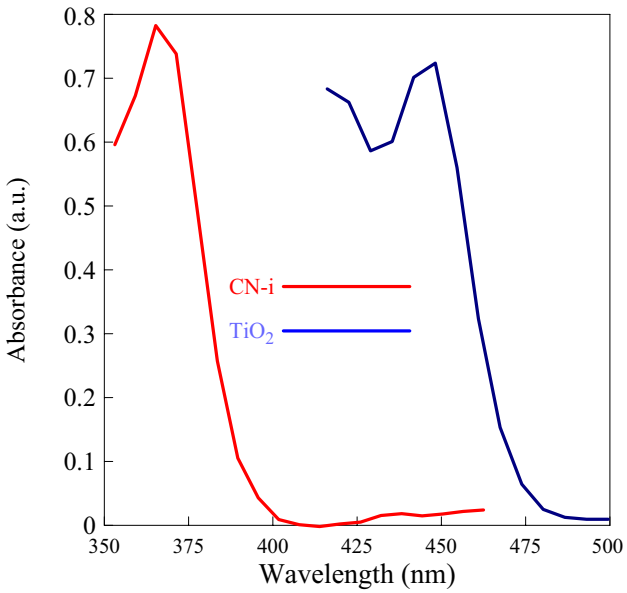


Fig. 3 Absorption spectra of CN-i and TiO_2 thin films.

Table I Comparison of TiO_2 and TiO_2/ CN-i double films

Material	ρ (Ω.cm)	n (cm^{-3})	μ (cm^2/Vs)
TiO_2	4.451×10^{-2}	7.385×10^{18}	2.8
TiO_2/ CN-i	1.983×10^{-5}	5.216×10^{19}	16.4

was increased considerably, ensuring a good photovoltaic conversion.

This finding suggested that electron transfer is becoming better and faster through binary structure (TiO_2 and CN-i) when compared with single film (TiO_2). The closely stacked binary layers showed a synergetic effect by adjusting the Fermi levels by leading more electrons to pass easily. To a large extent, the performance of the SCs is dictated by their efficiency in extracting the photogenerated charge, which is related to the charge carrier mobility in the photoactive layer.

In addition, Hall effect measurement (Accent HL5500pc) were obtained at room temperature. The resistivity (ρ) of the TiO_2/CN-i double films (1.983×10^{-5} Ω.cm) is much lower than that of TiO_2 film (4.451×10^{-2} Ω.cm) (Table I). Carrier concentration (n) and mobility (μ) values also show that the double layer device construction is completely in favor of the device in terms of performance.

Table I also compares the electrical properties of pristine TiO_2 and TiO_2/CN-i double-layer films. The reference TiO_2 film exhibits a resistivity of 4.45×10^{-2} Ω·cm, a carrier concentration of 7.38×10^{18} cm^{-3}, and electron mobility of 2.8 $cm^2{\cdot}V^{-1}{\cdot}s^{-1}$, which fall well within the typical ranges reported for spin-coated or sputtered TiO_2 electron transport layers in thin-film photovoltaic applications.[65–68]

Upon the incorporation of the ultrathin CN-i interlayer, the resistivity decreased dramatically by more than three orders of magnitude to 1.98×10^{-5} Ω·cm, accompanied by a significant increase in carrier concentration to 5.21×10^{19} cm^{-3} and an enhancement of electron mobility to 16.4 $cm^2{\cdot}V^{-1}{\cdot}s^{-1}$. Such simultaneous improvements in carrier density and mobility are comparable to, or exceed, values reported for TiO_2 modified with organic interlayers (e.g., PEI, conjugated molecules) or doped TiO_2 systems, where interface engineering has been shown to reduce transport barriers and suppress interfacial recombination.

The closely stacked binary layers showed a synergetic effect by leading more electrons to pass. A CN-i derivative, chosen as an organic semiconductor, includes a phenanthroimidazole ring as an electron donor and a cyano group as an electron acceptor, which are connected to each other by an imine bridge. The effects of the electron donor–acceptor groups and the long-conjugated system led to enhanced electron mobility, resulting in more efficient power output and higher efficiency.

In addition to these findings, ultra-high vacuum and complex equipment is not needed in photoelectron emission spectroscopy (PES) and photoconductivity measurements were also conducted (Fig. 4a, b). We conducted the measurements carried out in a vacuum (2×10^{-5} mbar) using a self-constructed system involving a laser-driven light source, white light source, monochromator, and Keithley electrometer (used as a voltage source and for electric current measurements). The same equipment was employed for photoconductivity measurements as in photoelectron emission spectroscopy.

The ionization energy was determined from the spectral dependence of photoelectron emission yield, identified as the threshold energy at which the yield increases rapidly. Photoemission yield $Y(h\nu)$ can be derived as:

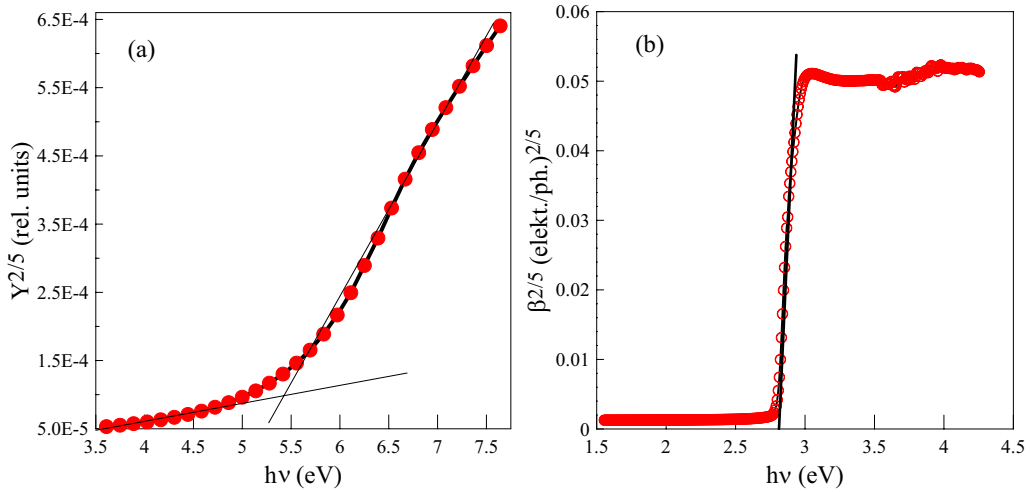


Fig. 4 The spectra for CN-i. (a) Photoelectron emission and (b) photoconductivity.

$$Y(h) = \frac{N(h)}{P(h\nu)} \tag{1}$$

where $N(h\nu)$ is the number of emitted electrons and $P(h\nu)$ is the number of incident photons with energy $h\nu$. Close to the threshold energy, the photoemission efficiency is directly related to the difference between the photon energy and the value of the ionization energy level; $Y(h) \propto (h\nu - 1)^{\frac{2}{5}}$. To obtain the ionization energy level value of the CN-i dye, the $Y(h\nu)^{2/5}$ dependence on photon energy was plotted (see Fig. 4a). It was found that after 5.44 eV, the photoemission yield increased linearly. This value is subsequently regarded as the ionization energy (I) level of CN-i (HOMO = −I = −5.44 eV).

When the energy gap and the ionization energy (I) level value was known, it was possible to calculate the electron affinity level value[69,70]:

$$EA = I - Eg. \tag{2}$$

The actual energy difference between the ionization energy level of the donor molecule and the electron affinity level of the acceptor molecule was found with the photoconductivity measurement of the bulk heterojunction (donor:acceptor) structure. To obtain the E_g value of the CN-i dye, the $\beta(h\nu)^{2/5}$ spectral dependence was plotted, as seen in Fig. 4b. The bandgap energy E_g value was determined by extrapolating the straight line portion of $\beta(h\nu)^{2/5}$ versus $h\nu$ plot as the threshold energy. Photoconductivity efficiency, $\beta(h\nu)$ is nonlinearly proportional to the difference between the photon energy and gap energy: $(h\nu) \propto (h\nu - Eg)^{2/5}$. In this case, the gap value was determined to be 2.77 eV, placing the electron affinity at 2.67 eV. This also refers to the LUMO energy level, LUMO = −2.67 eV. This obtained bandgap is too close to the value obtained from the UV–Vis absorption spectra at 2. 76 eV.

A black tape mask under standard global AM 1.5 solar conditions (see Fig. 5) was used to measure current density–voltage (J–V) characteristics (see Fig. 6) and the incident photon-to-current conversion efficiency (IPCE) spectra (see Fig. 7). The device at 100 mW/cm^2 showed the best performance, with a maximum photocurrent density (J_{sc}) of 27.5 mA/cm^2, an open circuit voltage (V_{oc}) of 0.96 V, and a fill factor (FF) of 69.10 %, yielding an overall cell efficiency (PCE) of 18.24%. For a precise comparison, $TiO_2/SiO_2/p$-Si and the illuminated devices were also fabricated under the same conditions; performance tests of $TiO_2/SiO_2/p$-Si resulted in the following respective values: J_{sc}, 11.52 mA/cm^2 and V_{oc}, 0.48, as summarized in Table II.

The efficiency of the the illuminated devices indicate that the phenanthroimidazole unit is an efficient electron donor. The short-circuit photocurrent density increased in the order of illumination at 100 mA/cm^2 > 50 mA/cm^2 > 25 mA/cm^2 > 15 mA/cm^2 > 10 mA/cm^2 because of the better light-harvesting ability of high illumination compared with low illumination. The TiO_2/SiO_2/Si device seemed to have the lowest photoconversion performance when we control the CN-i effect. The current of the TiO_2/CN-i/SiO_2/p-Si heterojunction exhibited more carrier transport through the

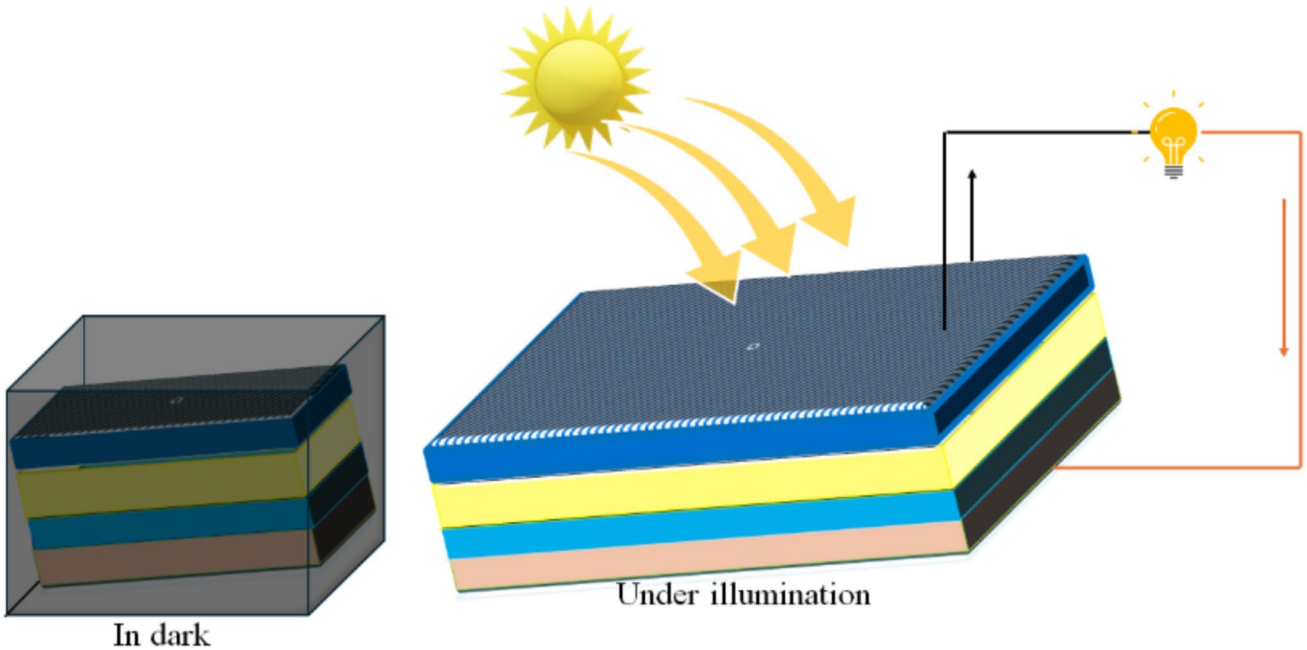


Fig. 5 Schematic setup of I–V measurement of SIS solar cells in dark conditiond and under illumination.

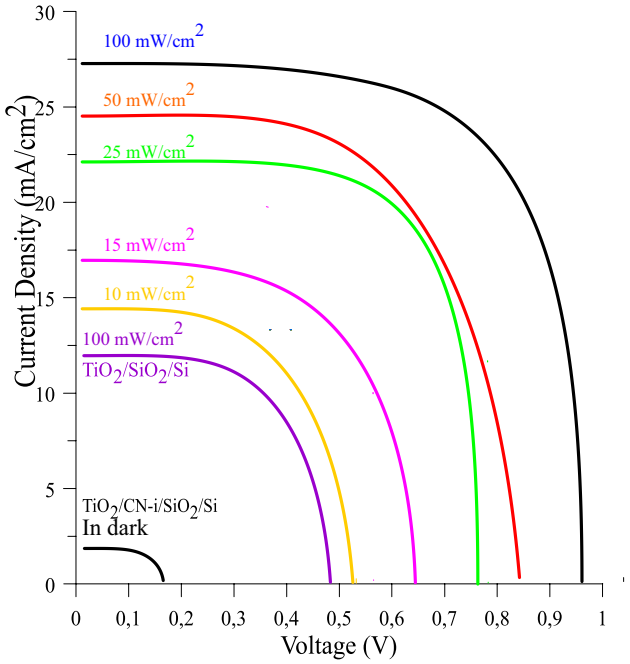


Fig. 6 Effect of illumination intensity on J–V characteristics of TiO_2/SiO_2/Si and TiO_2/CN-i/SiO_2/Si SIS solar cells (The dark J–V characteristics are included to highlight rectification behavior and interface-controlled transport in SIS devices).

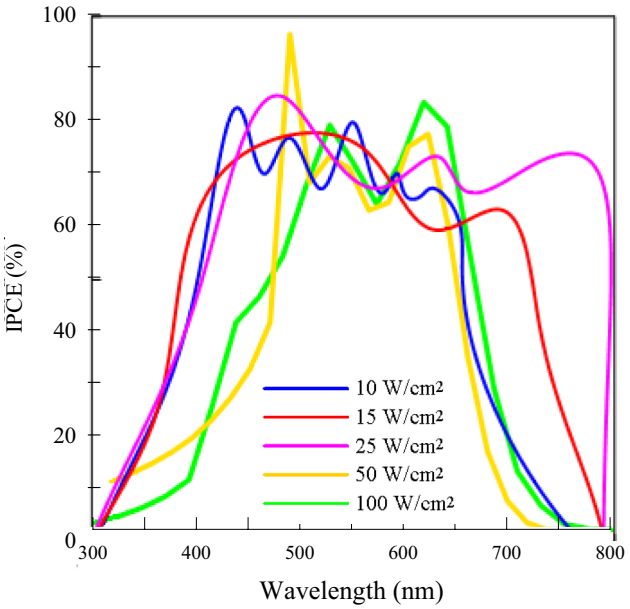


Fig. 7 Incident photon-to-current efficiency (IPCE)–wavelength characteristics of TiO_2/CN-i/SiO_2/Si under different illumination intensities.

ultrathin organic layer (CN-i) via direct tunneling phenomenon under AM 1.5 solar conditions according to the TiO_2/SiO_2/*p*-Si device. As long as it is exposed to light, sample areas covered with the transparent photoresist were capped by a shadow mask to prevent charge carrier generation outside the active area.

Table II Photovoltaic parameters of TiO_2/CN-i/SiO_2/Si and TiO_2/SiO_2/Si devices under different illumination intensities

SIS device	Illumination intensity (mW/cm^2)	J_{sc} (mA/cm^2)	V_{oc} (V)	FF (%)	PCE (%)
TiO_2/ CN-i/SiO_2/ Si	10	14.8	0.53	60.31	4.73
	15	16.8	0.65	60.21	6.57
	25	21.7	0.76	75.36	12.42
	50	23.8	0.84	66.04	13.20
	100 (1 sun)	27.5	0.96	69.10	18.24
	In dark	0.34	0.17	26.53	1.54
TiO_2/SiO_2/Si	100 (1 sun)	11.52	0.48	55.12	3.04

The meaningful change in the V_{oc} value of the SIS heterojunction can be attributed to the built-in potential increase, as confirmed by the increase in the threshold voltage under 100 mW/cm^2 illumination. This change in J_{sc} could be attributed to a reduction in the static charge carrier recombination and carrying out a better carrier transport with the CN-i contribution. Fill factor (FF) also increased from 55.12% to 69.10% after inserting the CN-i organic layer at the same illumination intensity; 100 mW/cm^2 (see Table II). The FF of the devices was calculated using Eq. 3 below[71]:

$$FF = \frac{P_{max}}{I_{sc}V_{oc}} \tag{3}$$

where P_{max} is the maximum power delivered by the device. The efficiencies of the SIS heterojunction device are calculated as in Eq. (4):

$$\eta = \frac{V_{OC}J_{SC}FF}{P_{in}}x100\% \tag{4}$$

Where P_{in}, input power; a particular value of current and voltage, respectively. The PCEs for illumination at 10 mW/cm^2 and 100 mW/cm^2 in the TiO_2/CN-i/SiO_2/Si and TiO_2/SiO_2/Si devices were 4.73% and 18.24%, respectively. The significant difference for PCE could be ascribed to the improved FF, J_{sc}, and V_{oc} for the SIS heterojunction compared with the conventional TiO_2/SiO_2/Si junction.

Although the literature on experimental SIS devices with ultrathin insulating interlayers remains limited compared with conventional *p–n* and heterojunction PV technologies, both experimental and simulation studies indicate that SIS- and tunnel-oxide-based structures can support moderately high efficiencies when designed for optimized interface energetics. For example, simulation work on TiO_2/insulator/Si SIS structures reports that careful control of the insulating

layer and band alignment can yield projected efficiencies in excess of 20–30% under ideal conditions, with high open-circuit voltage and fill factor resulting from favorable energy-level offsets and reduced recombination.[72] It should also be noted that other advanced silicon-based technologies such as tunnel oxide passivated contact (TOPCon) and heterojunction technology (HJT) cells—which also leverage ultrathin interfacial and passivating layers—have achieved certified efficiencies in the mid-20% range (e.g., ~26–27% for high-performance crystalline silicon cells in recent reports).[73]

Wenas et al., demonstrated a remarkable efficiency for a ZnO-SiO_2-Si SIS-type SC at 25%,[44] in addition to some SIS-type solar cells' efficiencies recorded as: 6.979% for $n+$ITOSiO_2-n-Si, 10.8% for ITO-SiO_x-n-Si devices. Untila and his coworkers reported many studies on SIS-type solar cells. In their studies recorded between 2015 and 2020, they achieved an efficiency of 8.3% for a AZO/($nn+$)Cz-Si/In_2O_3:F bifacial heterojunction solar cell and an efficiency of 16.6% for the ITO/SiO_x/n-Si heterojunction solar cell. These are motivating figures for SIS-type SCs and undeniable values on a laboratory scale. The 100 mW/cm^2 value we obtained is far above the average, based on the reported studies,[44–49,59] and is a solar cell that should be evaluated by making evaluating modifications for the possibility of achieving higher efficiency. In 2022, Kumar et al. reported an SIS-type SC of n-MoS_2/p-Si and n-MoS_2/AlN/p-Si heterojunctions-based photodetectors. The recorded responsivities for both n-MoS_2/p-Si and n-MoS_2/AlN/p-Si heterojunctions were found to be 0.3378 AW^{-1} and 1.865 AW^{-1} for visible radiation (532 nm) and 0.1245 AW^{-1} and 1.4743 AW^{-1} for near infrared (NIR) radiation (1064 nm), respectively. A drastic decrease in response time (rise time and decay time) was observed with the insertion of an ultrathin insulating AlN layer. The higher current in the SIS heterojunction evaluated was ascribed to the carrier tunneling mechanism through the ultrathin insulating layer.[74] The role of tunneling through ultrathin insulating layers in solar cell architectures has been extensively discussed in the literature. For example, modeling studies of semiconductor/insulator/semiconductor and tunnel-oxide passivated contact (TOPCon) solar cells show that the tunneling current across nanometer-scale oxide layers increases sharply as the insulator thickness decreases, and that efficient carrier collection with high fill factors requires sufficiently high tunneling probability through ultrathin oxide barriers.[75] Additionally, experimental investigations of carrier transport through ultrathin silicon-oxide layers demonstrate that for oxide thicknesses below about 1.2 nm, tunneling provides a dominant transport channel with reduced resistance, while thicker barriers lead to high series resistance and poor device performance, consistent with tunneling-dominated transport.[76] Similar tunneling effects have also been reported in other thin-film optoelectronic devices, where ultrathin insulating interlayers enhance photocurrent due to quantum tunneling of carriers across the barrier.[77] For example, early experimental SIS works using transparent conductive oxides on SiO_2/Si substrates have achieved moderate conversion efficiencies under AM 1.5G conditions, including 12.8–13% for ITO/SiO_2/p-Si and ITO/SiO_2/n-Si devices,[78] approximately 14.1% for SnO_2/SiO_2/n-Si heterojunctions,[78] around 8.5% for ZnO/SiO_2/n-Si,[78] and roughly 6.8% for AZO/SiO_2/p-Si structures.[78] These values are consistent with experimentally realized SIS cells employing TCO layers and intrinsic oxide barriers. In addition to these experimental reports, simulation studies indicate that optimized ZnO/SiO_2/Si SIS configurations can theoretically reach efficiencies above 25% under ideal device parameter regimes,[79] although such high values have yet to be widely realized experimentally. In this context, the 18.24% efficiency obtained in the present work with relatively simple interfacial engineering using a molecular CN-i layer and native oxide tunneling barrier is significantly above many traditional experimental SIS results and approaches the upper range predicted for optimized SIS designs. This comparison highlights the effectiveness of our interfacial energy level alignment and tunneling-assisted transport strategy in achieving high photovoltaic performance without requiring complex doping or multilayer processing.

The remarkably high V_{oc} value obtained here suggests that the CN-i interlayer effectively modifies the interfacial dipole and enhances the built-in potential beyond what is typically achieved in conventional TCO/SiO_2/Si SIS structures.

With this study, we can also say that CN-i are regenerating a sufficient built-in electric field for carrier separation and carrier transmission blocked by the insulating layer. For the TiO_2/CN-i/SiO_2/p-Si heterojunction photovoltaic device, the improved J–V curves due to well organized energy levels are probably enabling a smaller work function difference between the TiO_2 and Si substrate, which results in sufficient bending of the energy band of the silicon. Therefore, a built-in electric field is created to quickly separate the photogenerated carriers, which results in the improvement in FF and PCE values. Our results indicate that CN-i does not act as the primary photoactive absorber but rather plays a dual role as an interfacial electronic modifier and an efficient charge-transport/photoconductive layer.

Based on optical absorption, photoemission yield spectroscopy, photoconductivity measurements, and photovoltaic performance analysis, when CN-i does not primarily function as the main photoactive absorber. Instead, it acts predominantly as an interfacial electronic modifier and photoconductive charge-transport layer, improving energy level alignment, enhancing carrier mobility, suppressing interfacial recombination, and thereby enabling the high V_{oc}, FF, and overall PCE observed in the SIS solar cells.

Such simultaneous improvements in V_{oc}, FF, and carrier mobility strongly suggest that CN-i modifies the interfacial dipole and reduces recombination losses at the $TiO_2/SiO_2/p$-Si interface.

On the other hand, incident photon-to-current conversion efficiency (IPCE) is the second most important analysis after current density-voltage (J–V) measurement for testing solar cells. The IPCE values show a significant upward trend and support the J–V characteristics within the 80–90% range and between 350 nm and 700 nm (Fig. 7). This phenomenon may be owing to the ideal energy gap between the LUMO level of the CN-i and the conduction band edge of TiO_2, resulting in an increase in electron injection efficiency. Especially at 10 mW/cm^2 illumination, the IPCE graph is dominant in the 400–600 nm range, while at 100 mW/cm^2 illumination, two major peaks (530 nm and 620 nm, in the infrared range) stand out (Fig. 7). The IPCE spectra (see Fig. 7) exhibit a broad and high photoresponse extending well beyond the absorption range of CN-i (≈350–420 nm), indicating that CN-i is not the dominant photoactive absorber in the device. If CN-i were the primary absorber, the IPCE enhancement would be restricted to the near-UV region; however, the observed broadband response confirms that the main photon harvesting originates from the Si substrate. The enhanced IPCE over the entire visible spectrum demonstrates that CN-i improves carrier collection efficiency rather than acting as an additional light absorber.

The other measurement to analyze photovoltaic performance, transient photocurrent measurements, performed on the device under different illuminations yielded considerable changes in the charge extraction dynamics (see Fig. 8). Where all normalized photocurrent transients display an extraction of the mobile charge carriers after about 5.0 µs, the device illuminated at different illuminations (as seen in Fig. 8) exhibited a much higher fraction of slower charge carriers. As the extraction photocurrent was notably extended to longer times, it can be concluded that a larger fraction of the trapped charge carriers is present in the low illuminated device.

The transient photocurrent as a function of the time and illumination-dependent current density measurements to investigate the mechanisms of charge dissociation and recombination process (details in Table II) showed that an organic additive in nanoscale thickness reconstructs the active layers with enhanced crystallinity, charge mobility, and carrier lifetime of organic semiconductors in the SIS device, which leads to improved photovoltaic performance (Figs. 6, 7, and 8).

The observed dependence of V_{oc} and FF on illumination intensity is interpreted as a signature of interface-limited transport rather than bulk-dominated nonideal recombination. At low illumination levels, carrier densities are insufficient to fully activate tunneling-assisted charge transfer

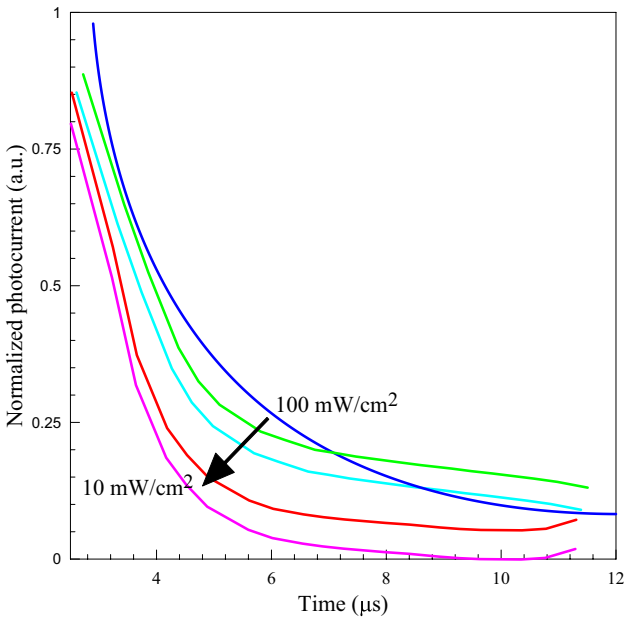


Fig. 8 Transient photocurrent traces of TiO_2/ CN-i/SiO_2/Si under different illuminations.

across the ultrathin interfacial layers, making interface recombination more pronounced and reducing both V_{oc} and FF. As the illumination intensity increases, enhanced carrier population promotes field-assisted tunneling and improves selective carrier extraction, leading to a systematic increase in V_{oc} and FF. The concurrent improvement of V_{oc}, FF, IPCE, and PCE with illumination intensity confirms that performance enhancement is governed by activated interfacial transport rather than bulk recombination losses.

This behavior is characteristic of SIS architectures and supports the dominance of interfacial transport and tunneling processes rather than uncontrolled recombination losses.

Conclusions

Herein, we introduce a new organic class of SIS solar cells to tailor the crystal growth of CN-i films from an inorganic content to an organic content design and accordingly increase the charge carrier mobility to accelerate electron transport and extraction. The mobility value of the double layer is eight times higher than that of TiO_2. This finding alone convinces us that this duo works well.

Introducing the 4-CN-phenyl group in the core unit serve as heteroatomic bridges for covalent planarization and this provides stronger electron-withdrawing character and allows for charge carrier mobility in contrast to core structural unit of the sole -imine group, thus increasing the HOMO energy

levels by tailoring the energy levels and enabling more efficient tunneling and more controlled current transport.

The SIS solar cells we obtained with this type of renewed design, using CN-i dye and tunneling dominant, phenanthroimidazole-imine compound containing amino groups and condensed with different aldehydes, were produced and tested in order to recognize and demonstrate in more detail the differences in their performance and carrier mechanisms compared with the $TiO_2/SiO_2/Si$ solar cells we used as reference. In general, CN-i dye-containing cells show better optical absorption and when compared with $TiO_2/SiO_2/Si$ solar cells: we found that it has higher absorption density and higher performance. This is an indicator of better charge transfer.

The results proved that it could perform better compared with standard SIS cell efficiency. As a result, there is a significant increase in the development of such OPV technologies, and we hope that this work will contribute to the current body of literature, which provides interesting and useful results with relatively low costs.

Acknowledgements This research received no external funding.

Authors Contributions Conceptualization: [Songül Fiat Varol]; Methodology: [Songül Fiat Varol],[Ziya Merdan]; Formal analysis and investigation: [Songül Fiat Varol],[Seçil Çelik Erbaş], [Sibel Gülle]; Writing—original draft preparation: [Songül Fiat Varol]; Writing—review and editing: [Songül Fiat Varol],[Seçil Çelik Erbaş], [Sibel Gülle]; Resources: [Songül Fiat Varol],[Ziya Merdan],[Seçil Çelik Erbaş], [Sibel Gülle]; Supervision: [Songül Fiat Varol],[Ziya Merdan].

Funding Open access funding provided by the Scientific and Technological Research Council of Türkiye (TÜBİTAK).

Data Availability The data that has been used is confidential.

Conflict of Interest The authors declare that they have no known competing financial interests or personal relationships that could have appeared to influence the work reported in this paper.

Ethics Approval This study does not contain any studies with human or animal subjects performed by any of the authors.

Open Access This article is licensed under a Creative Commons Attribution 4.0 International License, which permits use, sharing, adaptation, distribution and reproduction in any medium or format, as long as you give appropriate credit to the original author(s) and the source, provide a link to the Creative Commons licence, and indicate if changes were made. The images or other third party material in this article are included in the article's Creative Commons licence, unless indicated otherwise in a credit line to the material. If material is not included in the article's Creative Commons licence and your intended use is not permitted by statutory regulation or exceeds the permitted use, you will need to obtain permission directly from the copyright holder. To view a copy of this licence, visit http://creativecommons.org/licenses/by/4.0/.

References

1. A. Khasbaatar, Z. Xu, J.-H. Lee, G. Campillo-Alvarado, C. Hwang, B.N. Onusaitis, and Y. Diao, From solution to thin film: molecular assembly of π-conjugated systems and impact on (Opto)electronic properties. *Chem. Rev.* 123(13), 8395–8487 (2023).
2. X. Ren, J. Li, R.J. Holmes, P.I. Djurovich, S.R. Forrest, and M.E. Thompson, Ultrahigh energy gap hosts in deep blue organic electrophosphorescent devices. *Chem. Mater.* 16(23), 4743–4747 (2004).
3. S. Sayin, S. Fiat Varol, Z. Merdan, and S. Eymur, Synthesis of isoniazid substituted pyrene (PINHy), and investigation of its optical and electrochemical features as tunable/flexible OLEDs. *J Mater Sci: Mater Electron* 28, 13094–13100 (2017).
4. S. Fiat Varol, S. Sayin, S. Eymur, Z. Merdan, and D. Unal, Optical performance of efficient blue/near UV nitropyridine-conjugated anthracene (NAMA) based light emitting diode. *Org Electron* 31, 25–30 (2016).
5. S. Fiat Varol, S. Sayin, and Z. Merdan, Optimization of HIL-HTL-free naphthalimide: isoquinoline TEOLEDs with BZO top electrode. *Solid State Electron* 209, 108755 (2023).
6. G. Sauvé, Photovoltaics Beyond Silicon, Development of active layer materials for solution-processable organic photovoltaics (Elsevier, 2024) p.255-301.
7. B. Zhang, M. He, C. Ge, K. Lin, X. Gao, and Q. Zhang, Degradable heteroaromatic polyazomethines for organic field-effect transistor applications. *Dyes Pigm.* 228, 112239 (2024).
8. B. Kulyk, S. Taboukhat, H. Akdas- Kilig, J.-L. Fillaut, M. Karpierz, and B. Sahraoui, Tuning the nonlinear optical properties of BODIPYs by functionalization with dimethylaminostyryl substituents. *Dyes Pigm* 137, 507–511 (2017).
9. M. Idris, C. Coburn, T. Fleetham, J. Milam-Guerrero, P.I. Djurovich, S.R. Forrest, and M.E. Thompson, Phenanthro[9,10-*d*]triazole and imidazole derivatives: high triplet energy host materials for blue phosphorescent organic light emitting devices. *Mater. Horiz.* 6, 1179 (2019).
10. W.-C. Chen, G.-F. Wu, Y. Yuan, H.-X. Wei, F.-L. Wong, Q.-X. Tong, and C.-S. Lee, A meta-molecular tailoring strategy towards an efficient violet-blue organic electroluminescent material. *RSC Adv.* 5(23), 18067 (2015).
11. J. Xiang, X. Cai, X. Lou, G. Feng, X. Min, W. Luo, B. He, C.C. Goh, L.G. Ng, J. Zhou, Z. Zhao, B. Liu, and B.Z. Tang, Biocompatible green and red fluorescent organic dots with remarkably large two-photon action cross sections for targeted Cellular imaging and real-time intravital blood vascular visualization. *ACS Appl. Mater. Interfaces* 7(27), 14965 (2015).
12. Z. Wang, P. Lu, S. Chen, Z. Gao, F. Shen, W. Zhang, Y. Xu, H.S. Kwok, and Y. Ma, Phenanthro [9,10-d] imidazole as a new building block for blue light emitting materials. *J. Mater. Chem.* 21, 5451–5456 (2011).
13. Z. Gao, Z. Wang, T. Shan, Y. Liu, F. Shen, Y. Pan, H. Zhang, X. He, P. Lu, B. Yang, and Y. Ma, High-efficiency deep blue, fluorescent emitters based on phenanthrol [9,10-d]imidazole substituted carbazole and their applications in organic light emitting diodes. *Org. Electron.* 15, 2667–2676 (2014).
14. Z. Gao, Y. Liu, Z. Wang, F. Shen, H. Liu, G. Sun et al., High-efficiency violet-light emitting materials based on phenanthrol [9,10-d]imidazole. *Chem A Eur J* 19, 2602–5 (2013).
15. G. Tian, W. Liang, Y. Chen, N. Xiang, Q. Dong, J. Huang, and J.H. Su, A novel spiroannulated host based on carbazole with good thermal stability and high triplet energy for efficient blue and green phosphorescent organic light emitting diodes. *Dye Pigm* 126, 296–302 (2016).

16. S. Ashok, P.P. Sharma, and S.J. Fonash, Spray-deposited ITO–Silicon SIS heterojuction solar cells. *Electron Devices IEEE Trans* 27, 725–730 (1980).
17. K. Dasgupta, K. Chowdhury, A. Mondal, S. Ray, and U. Gangopadhyay, Advancement and challenges for schottky barrier MIS/SIS solar cells: a review. *Trans. Indian Natl. Acad. Eng.* 7, 13–28 (2022).
18. A. Simaschevici, D. Serban, L. Bruc, Solar Cells on the Base of Semiconductor-Insulator- Semiconductor Structures, by Ed. Leonid A. Kosyachenko. (IntechOpen, 2011) p. 299-332.
19. Shewchun, R. Singh, MA. Green Theory of metal insulator semiconductor solar cells. J Appl Phys 48, 765 (1977).
20. Y. Zou, Y. Zhou, Y. Xi, H. Li, X. Tian, Y. Huang, L. Zhu, and X. Xu, Surface field effect probed by THz emission in lead-free perovskite $CsSnBr_3$ films and $CsSnB_r3/Si_O2$/Si heterojunction. *Surf. Inter.* 46, 104046 (2024).
21. H.-W. Fang, T.-E. Hsieh, and J.-Y. Juang, Influences of SiO_x layer thickness on the characteristics of In-Zn-O/SiO_x/*n*-Si hetero-junction structure solar cells. *Surf. Coat. Technol.* 231, 214–218 (2013).
22. F.A. Noor, F. Oktasendra, E. Sustini, and K. Khairurrijal, The effects of insulator thickness and substrate doping density on the performance of ZnO/SiO_2/n-Si solar cells. *Mater. Technol.* 33(14), 865–871 (2018).
23. A. Kumar, K. Kumar, and V. Krishnan, Sunlight driven methanol oxidation by anisotropic plasmonic Au nanostructures supported on amorphous titania: Influence of morphology on photocatalytic activity. *Mater. Lett.* 245, 45–48 (2019).
24. L.X. Sang, Y.X. Zhao, and C. Burda, TiO_2 nanoparticles as functional building blocks. *Chem. Rev.* 114, 9283–9318 (2014).
25. A. Kumar, V. Sharma, S. Kumar, A. Kumar, and V. Krishnan, Towards utilization of full solar light spectrum using green plasmonic Au-TiO_x photocatalyst at ambient conditions. *Surf. Interfaces* 11, 98–106 (2018).
26. P. Karuppasamy, N.R.-N. Nisha, A. Pugazhendhi, S. Kandasamy, and S. Pitchaimuthu, An investigation of transition metal doped TiO_2 photocatalysts for the enhanced photocatalytic decoloration of methylene blue dye under visible light irradiation. *J. Environ. Chem. Eng.* 9, 105254 (2021).
27. X. Chen, and S.S. Mao, Titanium dioxide nanomaterials: synthesis, properties, modifications, and applications. *Chem. Rev.* 107, 2891–2959 (2007).
28. L. Zheng, K. Hu, F. Teng, and X. Fang, Novel UV-visible photodetector in photovoltaic mode with fast response and ultrahigh photosensitivity employing Se/TiO_2 nanotubes heterojunction. *Small* 13, 1602448 (2017).
29. H. Zhang, J. Liu, T. Xu, W. Ji, X. Zong (2023) Recent advances on small band gap semiconductor materials (≤ 2.1 eV) for solar water splitting. Catalyst 13(4): 728
30. S. Gülle, S.Ç. Erbaş, and A. Uzel, Synthesis and spectroscopic studies of phenanthroimidazole-imine derivatives and evaluation of their antioxidant activity. *J. Fluoresc.* 28, 217–223 (2018).
31. Y.F. Sun, and Y.P. Cui, The synthesis, structure and spectroscopic properties of novel oxazolone-, pyrazolone-and pyrazoline-containing heterocycle chromophores. *Dye Pigm* 81, 27–34 (2009).
32. Y. Baek, X. Li, N. Kim, C.E. Park, T.K. An, J. Kim, and S.H. Kim, A critical role of amphiphilic polymers in organic–inorganic hybrid sol–gel derived gate dielectrics for flexible organic thin-film transistors. *J. Mater. Chem. C* 7, 11612–11620 (2019).
33. Y. Hu, D.X. Cao, A.T. Lill, L. Jiang, C.A. Di, X. Gao, H. Sirringhaus, and T.Q. Nguyen, Effect of alkyl-chain length on charge transport properties of organic semiconductors and organic field-effect transistors. *Adv. Electron. Mater.* 4, 1800175 (2018).
34. K. Wang, H. Chen, T. Niu, S. Wang, X. Guo, and H. Wang, Dopant-free hole transport materials with a long alkyl chain for stable perovskite solar cells. *Nanomater.* 9, 935 (2019).
35. A. Can, A. Facchetti, and H. Usta, Indenofluorenes for organic optoelectronics: the dance of fused five- and six-membered rings enabling structural versatility. *J. Mater. Chem. C* 10, 8496–8535 (2022).
36. Z. Li, Y. Lin, J.L. Xia, H. Zhang, F. Fan, Q. Zeng, D. Feng, J. Yin, and S.H. Liu, Synthesis of novel diarylethene compounds containing two imidazole bridge units and tuning of their optical properties. *Dye Pigm* 90, 245–252 (2011).
37. J. Yuan, Z. Li, M. Hu, S. Li, S. Huang, J. Yin, and S.H. Liu, Synthesis and photochromic properties of imidazole-based diarylethenes. *Photochem. Photobiol. Sci.* 10, 587–591 (2011).
38. J. Kulhanek, and F. Bures, Imidazole as a parent π-conjugated backbone in charge-transfer chromophores. *Beilstein J. Org. Chem.* 8, 25–49 (2012).
39. X.-W. Zhu, D. Luo, X.-P. Zhou, and D. Li, Imidazole-based metal-organic cages: synthesis, structures, and functions. *Coord. Chem. Rev.* 455, 214354 (2022).
40. R. Francke, and R.D. Little, Optimizing electron transfer mediators based on arylimidazoles by ring fusion: synthesis, electrochemistry, and computational analysis of 2-Aryl-1-methylphenanthro[9,10-*d*]imidazoles. *J. Am. Chem. Soc.* 136, 427–435 (2014).
41. A.K. Padhy, B. Chetia, S. Mishra, A. Pati, and P.K. Iyer, Imidazole derivatives as the organic precursor of ZnO nano particle. *Tetrahedron Lett.* 51, 2751–2753 (2010).
42. S.M. Chen, M. Gao, X.H. Fang, and Z.Q. Ma, Modifications and multiple roles of graphene film in SIS structural solar cells. *Sol. Energy* 122, 658–666 (2015).
43. K. Ellmer, A. Klein, B.Rech, ZnO and its applications. Transparent conductive zinc oxide (Springer, 2008)
44. W.W. Wenas, and S. Riyadi, Carrier transport in high-efficiency ZnO/SiO_2/Si solar cells. *Sol. Energy Mater. Sol. Cells* 90, 3261–3267 (2006).
45. M. Zhang, X. Ga, A. Barra, P. Chang, L. Huang, R. Hellwarth, and J.G. Lu, Core-shell structured Si/ZnO photovoltaics. *Mater. Lett.* 140, 59–63 (2015).
46. S.-L. Chung, and C.-M. Wang, Solution combustion synthesis of TiO_2 and its use for fabrication of photoelectrode for dye-sensitized solar cell. *J. Mater. Sci. Technol.* 28, 713–722 (2012).
47. I. Iwantono, F. Anggelina, S.K.-M. Saad, M.Y.-A. Rahman, and A.A. Umar, Influence of Ag ion adsorption on the photoactivity of ZnO nanorods for dye-sensitized solar cell application. *Mater Express* 7(4), 312–318 (2017).
48. H. Jiang, X. Yang, Z. Wen, K. Ge, F. Li, J. Chen, Y. Xu, D. Song, and J. Chen, Considerably improved photovoltaic performances of ITO/Si heterojunction solar cells by incorporating hydrogen into near-interface region. *IEEE J. Photovolt.* 12(5), 1102–1108 (2022).
49. O. Malik, W FJ. De la Hidalga, I C,. Zuniga, T G. Ruiz, Efficient ITO–Si solar cells and power modules fabricated with a low temperature technology: results and perspectives. J Non-Cryst Solid. 354, 2472–2477 (2008).
50. G.G. Untila, T.N. Kost, A.B. Chebotareva, and E.D. Kireeva, Contact resistance of indium tin oxide and fluorine-doped indium oxide films grown by ultrasonic spray pyrolysis to diffusion layers in silicon solar cells. *Sol Energy Mater Sol Cell.* 137, 26–33 (2015).
51. G.G. Untila, T.N. Kost, and A.B. Chebotareva, Bifacial 8.3%/5.4% front/ rear efficiency ZnO:Al/n-Si heterojunction solar cell produced by spray pyrolysis. *Sol Energy* 127, 184–197 (2016).
52. G.G. Untila, T.N. Kost, and A.B. Chebotareva, Fluorine-doped ZnO (FZO) films produced by corona-discharge-assisted ultrasonic spray pyrolysis and hydrogenation as electron-selective

contacts in FZO/SiOx/p-Si heterojunction crystalline silicon solar cells with 11.7% efficiency. *Sol Energy* 179, 352–362 (2019).
53. G.G. Untila, T.N. Kost, and A.B. Chebotareva, ITO/SiOx/n-Si heterojunction solar cell with bifacial 16.6%/14.6% front/rear efficiency produced by ultrasonic spray pyrolysis: effect of conditions of SiOx growth by wet-chemical oxidation. *Sol Energy* 204, 395–405 (2020).
54. DL. Young, W. Nemeth, S. Grover, A. Norman, BG. Lee, P. Stradins, *IEEE 40th photovoltaic specialist conference (PVSC),* (2014) p. 1–5.
55. A. Saboor, S.M. Shah, and H. Hussain, Band gap tuning and applications of ZnO nanorods in hybrid solar cell: Ag-doped verses Nd doped ZnO nanorods. *Mater. Sci. Semicond. Process.* 93, 215–225 (2019).
56. X. Xu, C. Liu, Z. Sun, T. Cao, Z. Zhang, E. Wang, Z. Liu, and K. Liu, Interfacial engineering in graphene bandgap. *Chem. Soc. Rev.* 47, 3059–3099 (2018).
57. N. Sharma, M. Arif, S. Monga, M. Shkir, Y.K. Mishra, and A. Singh, Investigation of bandgap alteration in graphene oxide with different reduction routes. *Appl. Surf. Sci.* 513, 145396 (2020).
58. K. Dasgupta, S. Ray, A. Mondal, and U. Gangopadhyay, Review on different front surface modification of both n+-p-p+ and p+-n-n+ C- Si solar cell. *Mater Today Proc* 4(14), 12698–12707 (2017).
59. K. Kumar, A. Kumar, and D. Kaur, Improved power conversion efficiency in n-MoS_2/AlN/p-Si (SIS) heterojunction based solar cells. *Mater. Lett.* 277, 128360 (2020).
60. X. Jia, D. Zhong, Y. Ding, J. Zhao, Y. Fang, X. Zhang, D. Wang, and Z. Zhang, Design of highly efficient 0D/1D TiO_2 photoanode for dye-sensitized solar cells by simple $TiCl_4$ pre-treatment of titanate nanotubes. *Optical Mater.* 152, 115482 (2024).
61. K. Yoshikawa, H. Kawasaki, W. Yoshida, T. Irie, K. Konishi, K. Nakano, T. Uto, D. Adachi, M. Kanematsu, H. Uzu, and K. Yamamoto, Silicon heterojunction solar cell with interdigitated back contacts for a photoconversion efficiency over 26%. *Nat. Energ.* 2, 17032 (2017).
62. S. Essig, M.A. Steiner, C. Allebe, J.F. Geisz, B. Paviet-Salomon, S. Ward, A. Descoeudres, V. LaSalvia, L. Barraud, N. Badel, A. Faes, J. Levrat, M. Despeisse, C. Ballif, P. Stradins, and D.L. Young, Realization of GaInP/Si dual-junction solar cells with 29.8% 1-sun efficiency. *IEEE J. Photovolt* 6, 1012–1019 (2016).
63. H. Zhang, X. Zhang, C. Liu, S.T. Lee, and J. Jie, High-responsivity, high-detectivity, ultrafast topological insulator Bi_2Se_3/Silicon heterostructure broadband photodetectors. *ACS Nano* 10, 5113–5122 (2016).
64. L.A. García-Contrerasa, J.O. Flores-Floresa, J.Á. Arenas-Alatorreb, and J.Á. Chávez-Carvayarc, Synthesis, characterization and study of the structural change of nanobelts of TiO_2 ($H_2Ti_3O_7$) to nanobelts with anatase, brookite and rutile phases. *J. Alloys Compd.* 923, 166236 (2022).
65. D. Yang, P. Fu, F. Zhang, N. Wang, J. Zhang, and C. Li, High efficiency inverted polymer solar cells with room-temperature titanium oxide/ polyethylenimine films as electron transport layers. *J. Mater. Chem. A* 2, 17281 (2014).
66. A.A. Ahmad, L.A. Alakhras, Q.M. Al-Bataineh, and A. Telfah, Impact of metal doping on the physical characteristics of anatase titanium dioxide (TiO_2) films. *J. Mater. Sci. Mater. Electron.* 34, 1552 (2023).
67. M.I. Khan, and K.A. Bhatti, Rabia Qindeel, Hayat Saeed Althobaiti, Norah Alonizan, Structural, electrical and optical properties of multilayer TiO_2 thin films deposited by sol–gel spin coating. *Result. Phys.* 7, 1437–1439 (2017).
68. M. R. Islam, M.A. Zubair, M.S. Bashar, A.K.M.B. Rashid, Bi0.9Ho0.1FeO3/TiO2 Composite Thin Films: Synthesis and Study of Optical, Electrical and Magnetic Properties. Sci Rep. 26(9), 5205 (2019).
69. E. Louis, E. San-Fabián, M.A. Díaz-García, G. Chiappe, and J.A. Verges, Are electron affinity and ionization potential intrinsic parameters to predict the electron or hole acceptor character of amorphous molecular materials. *J. Phys. Chem. Lett.* 8, 2445–2449 (2017).
70. R. Grzibovskis, A. Polaks, and A. Vembris, Intrinsic photoconductivity spectral dependence as a tool for prediction of open-circuit voltage in organic solar cells. *Energies* 16, 6728 (2023).
71. R.A. Soref, Silicon-based optoelectronics. *Proc. IEEE* 81, 1687–1706 (1993).
72. A. Bouriche, C.-E. Benouis, M. Benhaliliba, and K. Dris, Optimizing semiconductor-insulator-semiconductor heterojunction engineering performance in a novel high-efficiency solar cell structure. *Periodica Polytechnica Chem. Eng.* 69(2), 204–218 (2025).
73. W. Shen, Y. Zhao, and F. Liu, Highlights of mainstream solar cell efficiencies in 2023. *Front. Energy* 18(1), 8–15 (2024).
74. K. Kumar, R. Yadav, S. Husale, P. Singh, and D. Kaur, "Ultrafast photoresponse in n-MoS_2/AlN/p-Si (SIS) heterojunction based visible to NIR photodetectors. *Sol. Ener. Mater. Sol. Cells* 246, 111942 (2022).
75. F.A. Noor, F. Oktasendra, E. Sustini, M. Abdullah, and K. Khairurrijal, A theoretical study on the performance of SnO_2/SiO_2/n-Si solar cells. *Material. Sci. Forum* 737, 1–8 (2013).
76. Z. Zhang, Y. Zeng, C.-S. Jiang , Y. Huang , M. Liao, H. Tong , M. Al-Jassim, P. Gao, C. Shoue, X. Zhoua, B. Yan, J. Ye, Carrier transport through the ultrathin silicon-oxide layer in tunnel oxide passivated contact (TOPCon) c-Si solar cells. *Sol. Ener. Mater.. Sol. Cell.*, 187 (2018).
77. C.H. Ji, J.Y. Lee, K.T. Kim, and S.Y. Oh, Enhanced photocurrent in organic photodetectors by the tunneling effect of a hafnium oxide thin film as an electron blocking layer. *RSC Adv.* 9, 29993 (2019).
78. O. Bethge, M. Nobile, S. Abermann, M. Glaser, and E. Bertagnolli, ALD grown bilayer junction of ZnO:Al and tunnel oxide barrier for SIS solar cell. *Sol. Energy Mater. Sol. Cells* 117, 178–182 (2013).
79. X.M. Song, C.Y. Ye, and Z.G. Huang, Optimization of SIS solar cells with ultra-thin silicon oxide layer. *Front. Ener. Res* 11, 1283196 (2023).

Publisher's Note Springer Nature remains neutral with regard to jurisdictional claims in published maps and institutional affiliations.